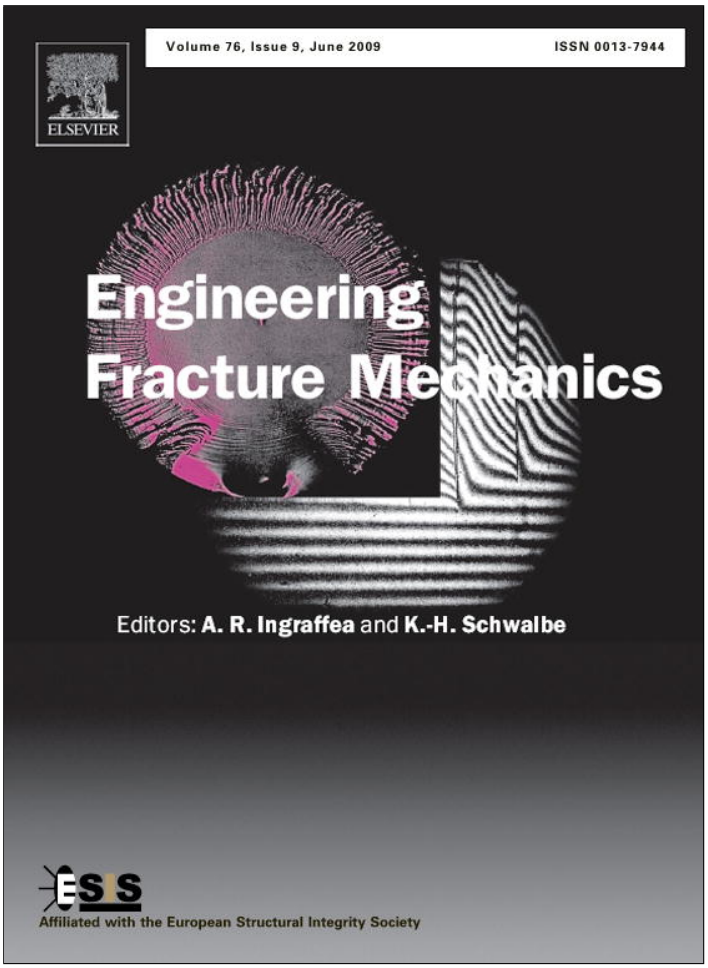

Engineering Fracture Mechanics 76 (2009) 1255–1267

Contents lists available at ScienceDirect

Engineering Fracture Mechanics

journal homepage: www.elsevier.com/locate/engfracmech

On fracture initiation toughness and crack sharpness for Mode II cracks

P. Trapper, K.Y. Volokh *

Faculty of Civil and Environmental Engineering, Technion-I.I.T., Haifa 32000, Israel

ARTICLE INFO

Article history:
Received 2 June 2008
Received in revised form 22 October 2008
Accepted 23 January 2009
Available online 5 February 2009

Keywords:
Fracture toughness
Crack
Sharpness
Failure
Hyperelasticity
Softening

ABSTRACT

Fracture toughness of brittle materials is calibrated in experiments where a sample with a preexisting crack is loaded up to a critical point of the onset of static instability. Experiments with ceramics, for example, exhibit a pronounced dependence of the toughness on the sharpness of the crack/notch: the sharper is the crack the lower is the toughness. These experimental results are not entirely compatible with the original Griffith theory of brittle fracture and Linear Elastic Fracture Mechanics which both ignore the crack sharpness.

To explain the experimental observations qualitatively we earlier considered Mode I cracks [Volokh KY, Trapper P. Fracture toughness from the standpoint of softening hyperelasticity. J Mech Phys Solids 2008;56:2459–72.] and in the present work we extend our considerations to Mode II cracks. We simulate pure shear of a thin plate with a small crack of a finite and varying sharpness. In simulations we introduce the failure energy as a limiter for the stored energy of the Hookean solid. The energy limiter induces softening, indicating material failure. Thus, elasticity with softening allows capturing the critical point of the onset of static instability of the cracked plate, which corresponds to the onset of the failure propagation at the tip of the crack. In numerical simulations we find that the magnitude of the fracture toughness can not be determined uniquely because it depends on the sharpness of the crack: the sharper is the crack the lower is the toughness.

Based on the obtained results we argue that a stable magnitude of the toughness of brittle materials can only be reached when a characteristic size of the crack tip is comparable with a characteristic length of the material microstructure, e.g. grain size, atomic distance etc. In other words, the toughness can be calibrated only under conditions where the hypothesis of length-independent continuum fails.

1. Introduction

Experiments on calibration of the fracture toughness in ceramics exhibit scattering of the results: the magnitude of the fracture toughness soundly depends on the sharpness of a *real* crack – see Bertolotti [3], Myers and Hillberry [25], Munz et al. [23], Wang et al. [38], Tsuji et al. [33], Gogotsi [11], Yosibash et al. [41], for example. These experimental results are not entirely compatible with the original Griffith [12] theory of brittle fracture where the real crack sharpness is of no influence. It is interesting that according to the Griffith equation of energy balance the finite crack sharpness is directly taken into account yet it does not affect the results.

The modern theory of Linear Elastic Fracture Mechanics (LEFM) also ignores sharpness of real cracks yet in a different way from the Griffith theory. LEFM considers 'mathematical' cracks with zero tip radius: Broberg [4], Hellan [13], Hertzberg [14], and Kanninen and Popelaar [19]. According to LEFM the critical shear stress on a plane with central crack of length $2a$ is given by

* Corresponding author.
E-mail address: cvolokh@technion.ac.il (K.Y. Volokh).

0013-7944/$ - see front matter © 2009 Elsevier Ltd. All rights reserved.
doi:10.1016/j.engfracmech.2009.01.016

$$p_{cr} = \frac{K_{IIc}}{\sqrt{\pi a}}, \tag{1}$$

where K_{IIc} is the Mode II fracture toughness or the critical stress intensity factor (SIF).

Formula (1) has been derived for a 'mathematical' crack and its practical application requires the experimental calibration of the fracture toughness, K_{IIc}. The latter is only possible in physical experiments with real cracks of finite sharpness. The contradiction between the mathematical assumption of singular cracks with infinite sharpness and physical reality of regular cracks with finite sharpness is evident.

There is an obvious mismatch between the experimental importance of the crack sharpness and its theoretical ignorance – see also Doremus [7]. To shed more light on this controversy we study the problem theoretically. We simulate failure of a cracked plate by using the softening hyperelasticity approach described in Section 2. Such an approach allows capturing the critical load on the cracked plate, which corresponds to the onset of static instability. Thus, our theoretical study is essentially a series of numerical experiments. The numerical experiments are not affected by the problems accompanying the physical experiments and because of that they can be a valuable source of additional information.

We plug the softening hyperelasticity models in ABAQUS and use very fine meshes to simulate small cracks with the varying sharpness or length in Section 3. We find that the crack sharpness affects the onset of plate failure and, consequently, the fracture toughness in perfect qualitative agreement with the physical experiments.

We discuss the results of our simulations and the classical theories of brittle fracture in Section 4. Particularly, we argue that the ignorance of the crack sharpness in the classical fracture theories is related to the energetic nature of these theories. The latter means that the energy balance, which is an integral equation, 'smears' the stress/strain concentration at the tip of the crack making the theory insensitive to the crack sharpness. The smearing appears explicitly in the original Griffith theory and it is implicit in LEFM. We also argue that the measurements of the fracture toughness can converge to stable values only in the cases where the radius of the crack tip is comparable with a characteristic size of the material microstructure, e.g. grain size, atomic distance etc., corresponding, for example, to the Emmerich [9] parameter λ_a that represents the minimum characteristic length scale round the point where the fracture begins. In other words, the toughness can be calibrated only under conditions where the hypothesis of continuum fails. The latter means, for example, that the measurements of the ceramics toughness with the notch radius significantly larger than the grain size may be hopeless in advance.

We note finally that the present work on Mode II cracks extends our previous work on Mode I cracks: Volokh and Trapper [37].

2. Softening hyperelasticity

2.1. Preliminary remarks

The existing continuum mechanics approaches for modeling material failure can be divided in two groups: surface and bulk models. The surface models, pioneered by Barenblatt [1], appear by name of Cohesive Zone Models (CZM) in the modern literature. The cohesive zone is a surface in a bulk material where displacement discontinuities occur. Thus, continuum is enhanced with discontinuities. The latter requires an additional constitutive description. Equations relating normal and tangential displacement jumps across the cohesive surfaces with the proper tractions define a specific CZM. There is a plenty of proposals of the 'cohesive' constitutive equations, for example, Dugdale [8], Rice and Wang [28], Tvergaard and Hutchinson [32], Xu and Needleman [40] and Camacho and Ortiz [5]. All these models are constructed qualitatively as follows: tractions increase, reach a maximum, and then approach zero with increasing separation. This scenario is in harmony with our intuitive understanding of the rupture process. Needleman [26] lifted the cohesive zone models to computational practice. Since then cohesive zone models are used increasingly in finite element simulations of crack tip plasticity and creep; crazing in polymers; adhesively bonded joints; interface cracks in bimaterials; delamination in composites and multilayers; fast crack propagation in polymers and etc. Cohesive zones can be inside finite elements or along their boundaries [6,40,2]. Crack nucleation, propagation, branching, kinking, and arrest are a natural outcome of the computations where the discontinuity surfaces are spread over the bulk material. This is in contrast to the traditional approach of fracture mechanics where stress analysis is separated from a description of the actual process of material failure. The CZM approach is natural for simulation of fracture at the internal material interfaces in polycrystals, composites, and multilayers. It is less natural for modeling fracture of the bulk because it leads to the simultaneous use of two material models for the same real material: one model describes the bulk while the other model describes the cohesive zones imbedded in the bulk. Such two-model approach is rather artificial physically. It seems preferable to incorporate a material failure law directly in the constitutive description of the bulk.

Remarkably, the first models of bulk failure – damage mechanics – proposed by Kachanov [17] and Rabotnov [27] for analysis of the gradual failure accumulation and propagation in creep and fatigue appeared almost simultaneously with the cohesive zone approach. The need to describe the failure accumulation, i.e. evolution of the material microstructure, explains why damage mechanics is very similar to plasticity theories including (a) the internal damage variable (inelastic strain), (b) the critical threshold condition (yield surface), and (c) the damage evolution equation (flow rule). The subsequent development of the formalism of damage mechanics [18,21,22,30] left its physical origin well behind the mathematical and computational techniques and eventually led to the use of damage mechanics for the description of any bulk failure. Theo-

retically, the approach of damage mechanics is very flexible and allows reflecting the physical processes triggering macroscopic damage at small length scales. Practically, the experimental calibration of damage theories is far from trivial because it is difficult to measure the damage parameter directly. The experimental calibration should be implicit and include both the damage evolution equation and criticality condition.

A physically motivated alternative to damage mechanics in the cases of failure related with the bond rupture has been considered by Gao and Klein [10], Klein and Gao [20] who showed how to mix the atomic/molecular and continuum descriptions in order to simulate material failure. They applied the Cauchy–Born rule linking micro- and macro-scales to empirical potentials, which include a possibility of the full atomic separation. The continuum-atomistic link led to the formulation of the macroscopic strain energy potentials allowing for the stress/strain softening and strain localization. The continuum-atomistic method is very effective at small length scales where purely atomistic analysis becomes computationally intensive. Unfortunately, a direct use of the continuum-atomistic method in macroscopic failure problems is not very feasible because its computer implementation includes a numerically involved procedure of the averaging of the interatomic potentials over a representative volume.

In order to bypass the computational intensity of the continuum-atomistic method while preserving its sound physical basis the softening hyperelasticity approach was proposed by Volokh [34], Volokh [35], Volokh [36]. The basic idea of the approach is to formulate an expression of the stored macroscopic energy, which includes the energy limiter – the average bond energy or the failure energy. Such a limiter introduces the strain softening, i.e. the material failure description, in constitutive equations of continuum mechanics automatically. The softening hyperelasticity approach is computationally simple yet physically appealing and its application to the simulation of the onset of the crack propagation in brittle solids is considered in the present work. It is interesting that the existence of an energy limiter has been observed by Rittel et al. [29] in experiments on adiabatic shear failure.

2.2. Energy limiter for a pair of particles

Let us start with the interaction of two particles (atoms, molecules etc) and let us choose, to be specific, the Lennard–Jones potential, ϕ, for the description of the particle interaction

$$\varphi(l) = 4\varepsilon((\sigma/l)^{12} - (\sigma/l)^{6}), \tag{2}$$

where l is the distance between particles ε and σ are the bond energy and length constants accordingly – Fig. 1.

Let L designate the distance between particles in a reference state and F is the one-dimensional deformation gradient. In the latter case we have

$$l = FL. \tag{3}$$

Substituting (3) in (2) we have

$$\varphi(F) = 4\varepsilon((\sigma/FL)^{12} - (\sigma/FL)^{6}). \tag{4}$$

Assuming that deformation increases to infinity we have

$$\varphi(F \to \infty) = 0. \tag{5}$$

On the other hand, we have at the reference state

$$\varphi_0 = \varphi(F = 1) = 4\varepsilon((\sigma/L)^{12} - (\sigma/L)^{6}). \tag{6}$$

In the absence of external loads the energy of the interaction tends to minimum and it is natural to choose the minimum energy state – equilibrium – at distance $L = \sqrt[6]{2}\sigma$ where no forces are acting between the particles. In the latter case we have

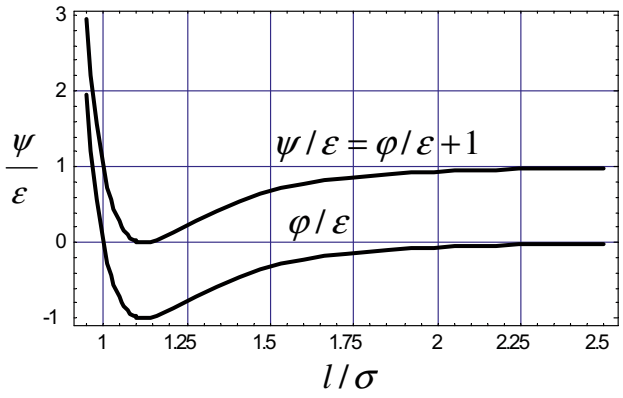

Fig. 1. Lennard–Jones potential.

$$\varphi_0 = -\varepsilon. \tag{7}$$

We notice that energy is negative in the equilibrium state according to the classical Lennard–Jones potential. The latter is inconvenient (in problems of solid mechanics) and we modify the classical LJ potential by shifting its reference energy to zero (Fig. 1)

$$\psi = \varphi + \varepsilon. \tag{8}$$

We further formalize the described energy shift as follows

$$\psi(F) = \varphi(F) - \varphi_0, \tag{9}$$

$$\varphi_0 = \min_L \varphi(F = 1). \tag{10}$$

Eqs. (9) and (10) are important in the subsequent consideration of assemblies of many particles.

It is important to emphasize that increasing deformation we cannot increase energy unlimitedly. The energy increase is limited

$$\psi(F \to \infty) = -\varphi_0 = \Phi = \text{constant}. \tag{11}$$

2.3. Energy limiter for assembly of particles

Now we extend all considerations for a pair of particles given in the previous subsection to large particle assemblies comprising solid bodies. Consider particles placed at $\mathbf{r}_i$ in the 3D space. Generally, the volumetric density of the total potential energy, i.e. the strain energy, can be written with account of two-particle interactions as follows

$$\frac{1}{2V}\sum_{i,j}\varphi(r_{ij}), \tag{12}$$

where $r_{ij} = |\mathbf{r}_{ij}| = |\mathbf{r}_i - \mathbf{r}_j|$ and V is the volume occupied by the system.

According to the Cauchy–Born rule [31,39], originally applied to the crystal elasticity, the current $\mathbf{r}_{ij}$ and initial (reference) $\mathbf{R}_{ij} = \mathbf{R}_i - \mathbf{R}_j$ relative positions of the same two particles can be related by the deformation gradient:

$$\mathbf{r}_{ij} = \mathbf{F}\mathbf{R}_{ij}, \tag{13}$$

where $\mathbf{F} = \partial\mathbf{x}/\partial\mathbf{X}$ is the deformation gradient of a generic material macro-particle of body Ω occupying position $\mathbf{X}$ at the reference state and position $\mathbf{x}(\mathbf{X})$ at the current state of deformation – Fig. 2.

Substituting (13) in (12) yields

$$\frac{1}{2V}\sum_{i,j}\varphi(r_{ij}) = \frac{1}{2V}\sum_{i,j}\varphi(r_{ij}(\mathbf{C})), \tag{14}$$

where $\mathbf{C} = \mathbf{F}^T\mathbf{F}$ is the right Cauchy–Green deformation tensor.

Direct application of (14) to analysis of material behavior can be difficult because of the large amount of particles. Gao and Klein [10], Klein and Gao [20] considered the following statistical averaging procedure

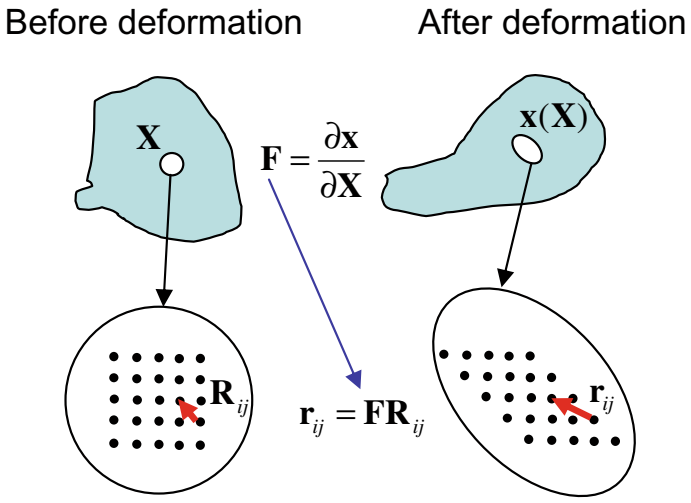

Fig. 2. Cauchy–Born rule.

$$\langle\varphi(l)\rangle = \frac{1}{V_0}\int_{V_0^*}\varphi(l)D_V dV, \tag{15}$$

$$l = r_{ij} = L\sqrt{\boldsymbol{\xi}\cdot\mathbf{C}\boldsymbol{\xi}} = L|\mathbf{F}\boldsymbol{\xi}|, \tag{16}$$

where $L = R_{ij} = |\mathbf{R}_i - \mathbf{R}_j|$ is the reference bond length; $\boldsymbol{\xi} = (\mathbf{R}_i - \mathbf{R}_j)/L$ is the reference bond direction; V_0 is the reference representative volume; $\varphi(l)$ is the bond potential (Lennard–Jones); D_V is the volumetric bond density function; and V_0^* is the integration volume defined by the range of influence of φ.

Now the average strain energy takes form

$$\langle\varphi(\mathbf{C})\rangle = \frac{1}{V_0}\int_{V_0^*} 4\varepsilon((\sigma/L\|\mathbf{C}\|)^{12} - (\sigma/L\|\mathbf{C}\|)^{6})D_V dV, \tag{17}$$

where

$$\|\mathbf{C}\| = \sqrt{\boldsymbol{\xi}\cdot\mathbf{C}\boldsymbol{\xi}}. \tag{18}$$

Analogously to the case of the pair interaction considered in the previous subsection – Eqs. (9) and (10) – we define the shifted strain energy, which is zero at the equilibrium reference state,

$$\psi(\mathbf{C}) = \langle\varphi(\mathbf{C})\rangle - \langle\varphi\rangle_0, \tag{19}$$

$$\langle\varphi\rangle_0 = \min_L\langle\varphi(\mathbf{C} = \mathbf{1})\rangle. \tag{20}$$

Analogously to (11), we can define the average bond energy by setting the unlimited increase of deformation

$$\Phi = \psi(\|\mathbf{C}\| \to \infty) = -\langle\varphi\rangle_0 = \text{constant}. \tag{21}$$

Thus, the average bond energy sets a limit for the energy accumulation. This conclusion generally does not depend on the choice of the particle potential and it is valid for any interaction that includes a possible particle separation – the bond energy.

2.4. Energy limiter for a solid

Contrary to the conclusion above traditional hyperelastic models of materials do not include the energy limiter. The stored energy of hyperelastic materials is defined as

$$\psi = W. \tag{22}$$

Here W is used for the strain energy of the intact material, which can be characterized as follows

$$\|\mathbf{C}\| \to \infty \Rightarrow \psi = W \to \infty, \tag{23}$$

where ||...|| is a tensorial norm.

In other words, the increasing strain increases the accumulated energy unlimitedly. Evidently, the consideration of only intact materials is restrictive and unphysical. The energy increase of a real material should be limited as it was shown above,

$$\|\mathbf{C}\| \to \infty \Rightarrow \psi = \Phi = \text{constant}, \tag{24}$$

where the average bond energy, Φ = constant, can be called the material failure energy.

Eq. (24) presents the fundamental idea of introducing a limiter of the stored energy in the elasticity theory. Such a limiter induces material softening, indicating material failure, automatically. The choice of the limited stored energy expression should generally be material-specific. Nonetheless, a somewhat universal formula [36] can be introduced to enrich the already existing models of intact materials with the failure description

$$\psi(W) = \Phi - \Phi\exp(-W/\Phi). \tag{25}$$

where $\psi(W = 0) = 0$ and $\psi(W = \infty) = \Phi$.

Formula (25) obeys condition $\|\mathbf{C}\| \to \infty \Rightarrow \psi(W(\mathbf{C})) = \Phi$ and, in the case of the intact material behavior, $W \ll \Phi$, we have $\psi(W) \approx W$ preserving the features of the intact material.

The constitutive equation can be written in the general form accounting for (25)

$$\boldsymbol{\sigma} = 2J^{-1}\mathbf{F}\frac{\partial\psi}{\partial\mathbf{C}}\mathbf{F}^T = 2J^{-1}\mathbf{F}\frac{\partial W}{\partial\mathbf{C}}\mathbf{F}^T\exp(-W/\Phi), \tag{26}$$

where $\boldsymbol{\sigma}$ is the Cauchy stress tensor; $J = \det\mathbf{F}$; and the exponential multiplier enforces material softening. Constitutive Eq. (26) is especially effective for incompressible soft materials undergoing finite deformations.

2.5. Hookean solid with failure

In the case of linear Hookean solid, which is of interest in the present study, we have for (25) and (26) accordingly

$$\psi = \Phi - \Phi \exp\{-(\lambda(\mathrm{tr}\boldsymbol{\varepsilon})^2/2 + \mu\boldsymbol{\varepsilon}:\boldsymbol{\varepsilon})/\Phi\}, \tag{27}$$

$$\boldsymbol{\sigma} = \frac{\partial\psi}{\partial\boldsymbol{\varepsilon}} = (2\mu\boldsymbol{\varepsilon} + \lambda(\mathrm{tr}\boldsymbol{\varepsilon})\mathbf{1})\exp\{-(\lambda(\mathrm{tr}\boldsymbol{\varepsilon})^2/2 + \mu\boldsymbol{\varepsilon}:\boldsymbol{\varepsilon})/\Phi\}, \tag{28}$$

where $\boldsymbol{\varepsilon}:\boldsymbol{\varepsilon} = \mathrm{tr}(\boldsymbol{\varepsilon}\boldsymbol{\varepsilon}^T)$; λ and μ are the Lame material constants and

$$\boldsymbol{\varepsilon} = (\mathbf{H} + \mathbf{H}^T)/2 \tag{29}$$

is the linear strain; $\mathbf{1}$ is the second-order identity tensor and $\mathbf{H} = \partial\mathbf{u}/\partial\mathbf{X}$ is the displacement, $\mathbf{u} = \mathbf{x} - \mathbf{X}$, gradient.

Though (25) presents a universal formula to introduce the average bond energy in consideration, it is by no means unique. It is possible, for example, to introduce the energy limiter for the linear isotropic Hookean solid in the following way [34,35]

$$\psi = \Phi - \Phi\left(1 + \sqrt{K/\Phi}\mathrm{tr}\boldsymbol{\varepsilon}\right)\exp\left\{-\sqrt{K/\Phi}\mathrm{tr}\boldsymbol{\varepsilon} - (\mu/\Phi)\mathbf{e}:\mathbf{e}\right\}, \tag{30}$$

$$\boldsymbol{\sigma} = \frac{\partial\psi}{\partial\boldsymbol{\varepsilon}} = 2\tilde{\mu}\boldsymbol{\varepsilon} + (\tilde{K} - 2\tilde{\mu}/3)(\mathrm{tr}\boldsymbol{\varepsilon})\mathbf{1}, \tag{31}$$

where

$$\mathbf{e} = \boldsymbol{\varepsilon} - (\mathrm{tr}\boldsymbol{\varepsilon})\mathbf{1}/3, \tag{32}$$

$$\tilde{\mu} = \mu\left(1 + \sqrt{K/\Phi}\mathrm{tr}\boldsymbol{\varepsilon}\right)\exp\left\{-\sqrt{K/\Phi}\mathrm{tr}\boldsymbol{\varepsilon} - (\mu/\Phi)\mathbf{e}:\mathbf{e}\right\}, \tag{33}$$

$$\tilde{K} = K\exp\left\{-\sqrt{K/\Phi}\mathrm{tr}\boldsymbol{\varepsilon} - (\mu/\Phi)\mathbf{e}:\mathbf{e}\right\}, \tag{34}$$

where $K = \lambda + 2\mu/3$ is the bulk modulus.

We emphasize again that the best form of the energy function can be material/problem-specific. It is important, however, that all possible forms should limit the energy increase. In what follows we will use both (27) and (30).

Remark 2.1. The so-called Cauchy–Born rule linking micro/nano- and macro- scales was originally formulated for crystal elasticity and it is widely used in modern continuum-atomistic methods. The Cauchy–Born rule is essentially an assumption of affinity of deformation of the physical particles within the representative small volumes of material. The applicability of the affinity hypothesis implies the applicability of the classical (nonlocal) continuum mechanics description of material. The continuum description of material proved itself for most materials at large length scales. It may fail, however, at small length scales where, for example, the atomic relaxation cannot be ignored. The latter cases are out of our consideration and we always assume that the local deformation is approximately affine.

Remark 2.2. It is important to realize that not all bonds between the material particles are of equal importance in (15). Only bonds presenting the weakest links define failure. In this sense it is probably better to call the energy limiter the failure energy rather than the average bond energy.

3. Finite element simulations

The purpose of the finite element analysis is to simulate the hydrostatic tension of a thin plate with the small elliptic and straight cracks – Fig. 3 – under the varying sharpness and length of the cracks.

For this purpose, we use the ABAQUS software where the stored energy functions (27) and (30) are plugged in. Henceforth, we call the material model based on (30) Softening Hyperelasticity 1 – SH1 – and on (27) Softening Hyperelasticity 2 – SH2. We consider the state of the plane stress for a square plate of size $d = 1600$ (units) with elastic constants $\lambda/\Phi = 75 \cdot 10^4/66$ and $\mu/\Phi = 90 \cdot 10^4/66$.

We use very fine meshes of linear triangles (CPS3) as shown in Fig. 4. The number of elements varies for various loading cases. We consider three series of simulations in the subsequent subsections.

3.1. Elliptic crack with varying sharpness

We start with the elliptic crack simulation with fixed length of $2a = 80$ (units) and varying sharpness, i.e. the 'width' half axes of the elliptic crack: $b = 1, 2, 3, 4, 5, 6, 7, 8$ (units). Table 1 presents the normalized critical shear stress for 8 cases of the crack sharpness.

Every case is simulated four times by using finite elements with different meshes and hyperelastic models. The results are very similar in all cases and their average is presented in Fig. 5a graphically.

It is clearly seen that the critical shear stress significantly depends on the sharpness of the elliptic crack. When the critical shear stress is known we can calculate the fracture toughness by using (1)

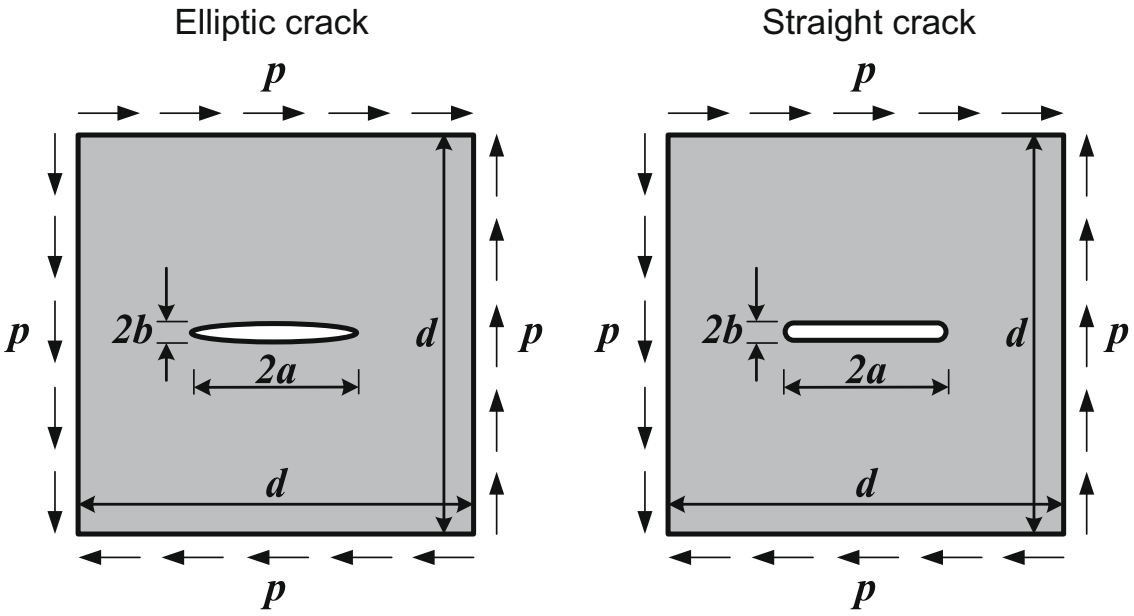

Fig. 3. Elliptic and straight cracks.

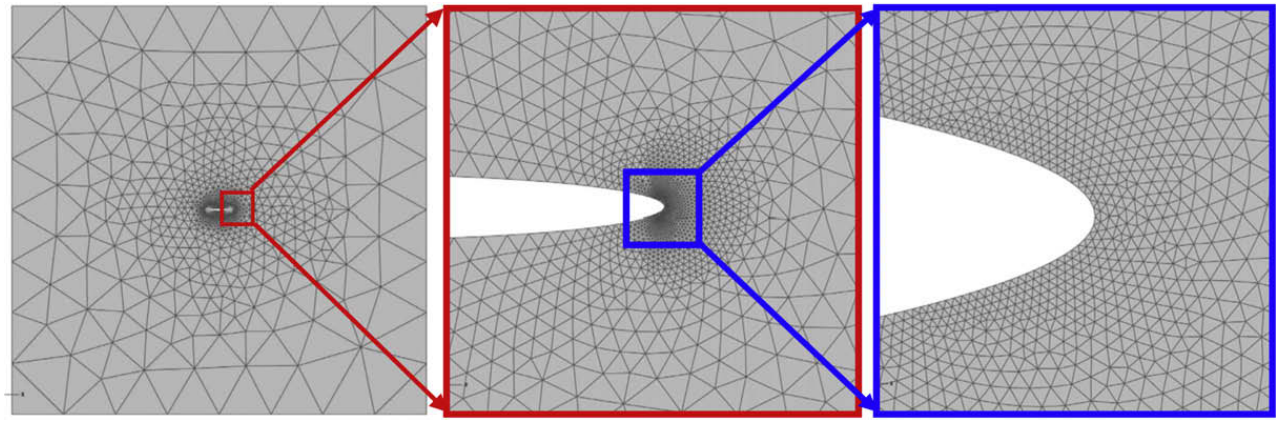

Fig. 4. Mesh of triangles.

Table 1
Normalized critical shear stress, p_{cr}/Φ, for elliptic crack with varying sharpness, and fixed length. SH1 – softening hyperelasticity model described by Eq. (30); SH2 – softening hyperelasticity model described by Eq. (27); second numbers designate the total number of finite elements for the half plate.

b/a	SH2		SH1	
1/40	4.2	4.0	4.2	4.0
	9804	13040	9804	13040
2/40	7.7	7.6	7.6	7.6
	7338	11144	7338	11144
3/40	10.9	11.0	10.7	10.8
	5428	7490	5428	7490
4/40	14.0	14.1	13.6	13.7
	3504	6960	3504	6960
5/40	16.1	16.2	15.3	15.5
	4854	6876	4854	6876
6/40	18.3	18.4	17.5	17.6
	4686	8444	4686	8444
7/40	20.6	20.8	19.4	19.5
	4592	8284	4592	8284
8/40	22.4	22.5	21.2	21.3
	4400	7860	4400	7860

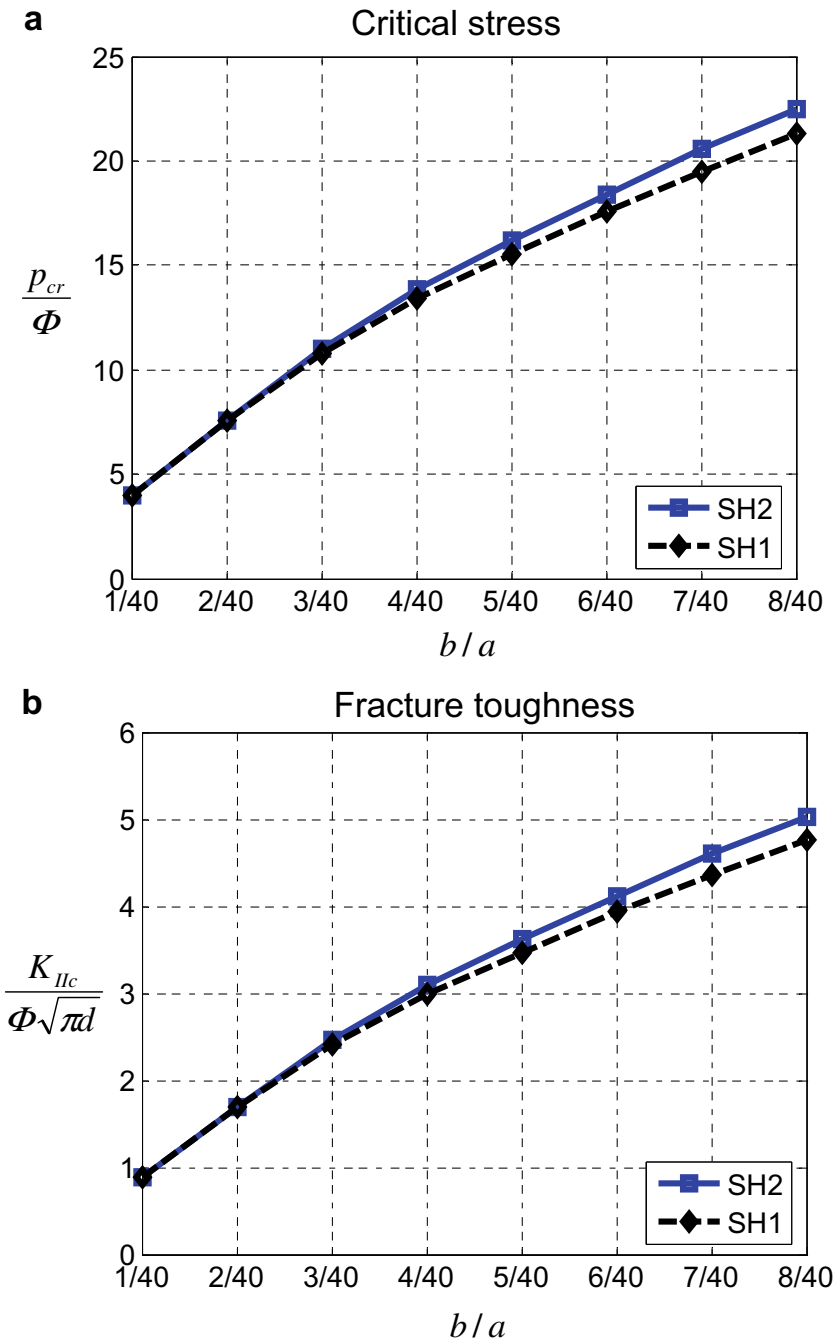

Fig. 5. Critical shear stress (a) and fracture toughness (b) for elliptic crack with varying sharpness and fixed length. SH1 – softening hyperelasticity model described by Eq. (30); SH2 – softening hyperelasticity model described by Eq. (27).

$$K_{IIc} = p_{cr}\sqrt{\pi a}. \tag{35}$$

The results of the calculations of the fracture toughness are presented in Fig. 5b. Evidently, no unique toughness can be determined for a crack with the fixed length. The numerical value of the toughness depends on the sharpness of the crack.

It is worth emphasizing that the "smallness" of the crack was checked by comparing the results of the present computations to the results of the similar computations with the enlarged plate. No significant difference in results has been found and we do not duplicate them here.

3.2. Straight crack with varying sharpness

The results similar to those presented in the previous subsection are also obtained for the straight crack, which is formed by two parallel lines joined by half-circles at the edges. Table 2 and Fig. 6 show the critical shear stresses and the fracture toughness for the case of the straight crack with the varying sharpness, i.e. width.

Table 2
Normalized critical shear stress, p_{cr}/Φ, for straight crack with varying sharpness and fixed length. SH1 – softening hyperelasticity model described by Eq. (30); SH2 – softening hyperelasticity model described by Eq. (27); second numbers designate the total number of finite elements for the half plate.

b/a	SH2		SH1	
0.5/40	7.2	7.2	6.6	6.5
	5264	12372	5264	12372
1/40	9.9	10.0	9.2	9.1
	4014	7906	4014	7906
1.5/40	11.8	11.9	11.0	11.0
	4076	7862	4076	7862
2/40	13.4	13.5	12.6	12.7
	3514	7028	3514	7028
2.5/40	14.7	14.8	13.9	13.9
	3236	6548	3236	6548
3/40	16.1	16.1	15.1	15.2
	3110	6038	3110	6038
3.5/40	16.9	17.0	16.0	16.1
	2894	5964	2894	5964
4/40	18.0	18.1	17.1	17.2
	2910	6020	2910	6020

Again, like in the case of the elliptic crack, no unique magnitude of the fracture toughness can be determined because it depends on the crack sharpness.

3.3. Straight crack with varying length

In addition to the analysis of the influence of the crack sharpness on the critical tension of a plate it is of interest to compare cracks with the equivalent sharpness and varying lengths. Such comparisons are presented in Tables 3 and 4 and Figs. 7 and 8. The obtained data clearly show that the crack length affects the critical tension in agreement with the LEFM only in the case of the cracks with the equivalent sharpness. The latter means that if the LEFM was calibrated for the sharpness corresponding to the middle curve in Figs. 7 and 8 then it could only predict the behavior of the cracks with the same sharpness and it would fail predicting the behavior of cracks with a different sharpness.

4. Discussion

The present work was motivated by a controversy between the observations of the influence of the crack sharpness on the fracture toughness in experiments and the ignorance of the crack sharpness in the classical theories of brittle fracture. To gain new insight into the controversy we numerically simulated the onset of the crack propagation in thin plates under the hydrostatic tension. The critical tension, when fracture starts, occurs when material fails at the tip of the crack. The failure is driven by the strain softening induced in the material constitutive model with the help of the energy limiter – the failure energy. The material (Hookean) model enhanced with the failure description was plugged in ABAQUS and crack simulations were performed on very fine meshes to examine the influence of the crack sharpness on the onset of fracture. Small elliptic and straight cracks were considered with the constant length and the varying tip curvature or the crack sharpness. It was observed that sharper cracks led to lower magnitudes of the critical tension. The latter, in turn, led to the lower magnitudes of the critical stress intensity factors – fracture toughness – in harmony with the experimental observations. The obtained results of the Mode II crack simulations are qualitatively similar to our simulations of Mode I cracks [37] and all conclusions below are equally applicable to the different crack modes.

Our observations are in agreement with the well-known Inglis [16] finding that the stress at the tip of an elliptic crack strongly depends on its sharpness. Assuming that the stress at the tip controls material strength it is possible to expect that the crack sharpness affects the onset of material failure. Such a scenario was considered by Inglis using linear elasticity. Comparing the approach of Inglis with the softening hyperelasticity approach used in the present work we should emphasize the difference between them. Inglis uses local – strength of materials – criteria of failure which are separated from the constitutive description of material. No global experiment on the calibration of the fracture toughness can be reproduced within the simplistic framework of strength of materials. The softening hyperelasticity approach is different. It allows tracking the global failure/instability of the structure with cracks due to the inclusion of the strain softening in the constitutive description of material. Thus, softening hyperelasticity allows reproducing the real physical experiments where the global instability/failure is observed. We should also note that Emmerich [9] revisited Inglis results by mixing continuum and atomistic arguments and arriving at similar conclusions. The Emmerich [9] work includes interesting discussions and an extensive list of references, which complements the references of the present work.

Why are the Griffith theory and LEFM ignorant of the crack sharpness? Such ignorance can be explained by the notion that the classical theories of brittle fracture are based on the energy balance considerations, which are integral and because of that they ‘smear’ the real stress/strain concentration at the tip of a real crack. The latter is explicit in the Griffith work

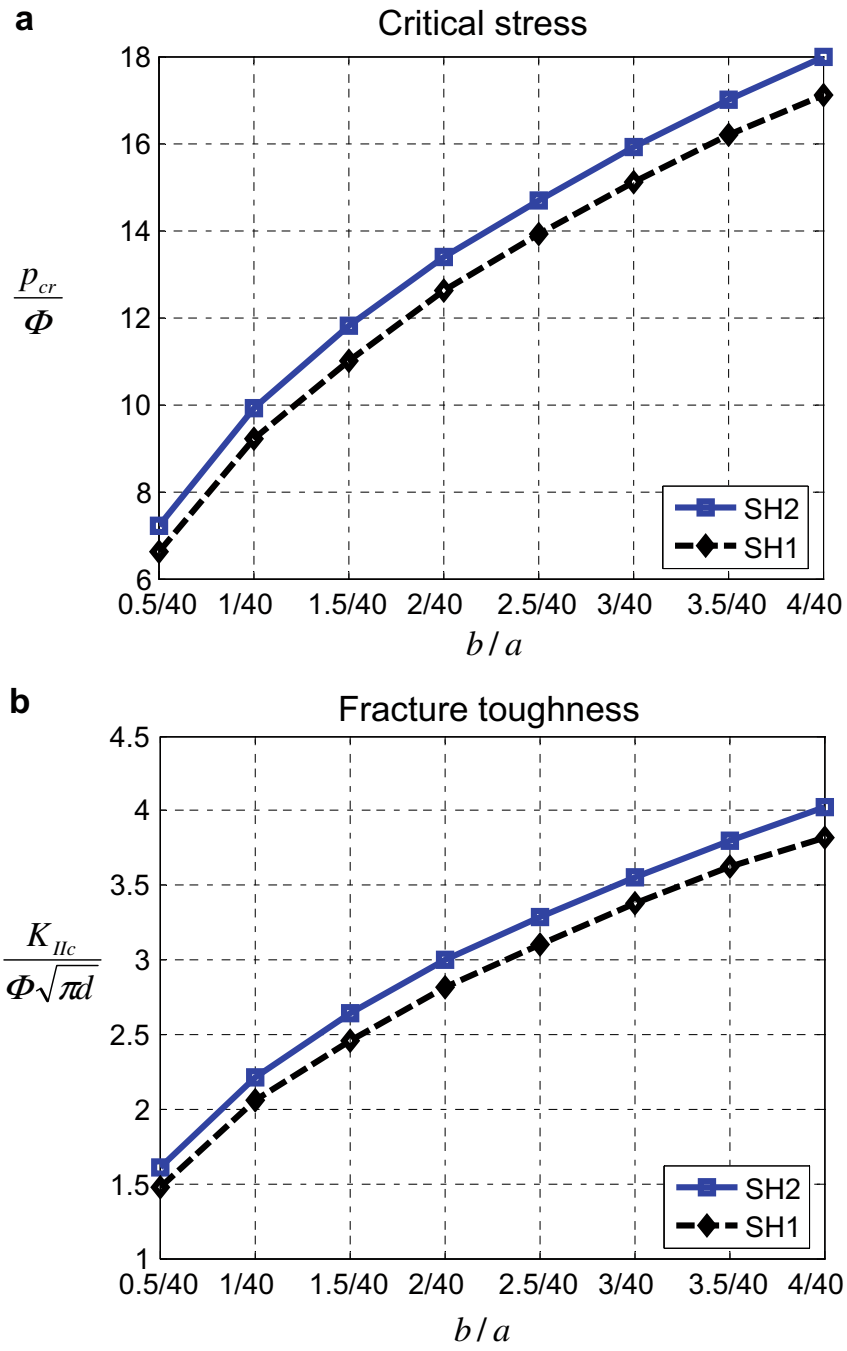

Fig. 6. Critical stress (a) and fracture toughness (b) for straight crack with varying sharpness and fixed length. SH1 – softening hyperelasticity model described by Eq. (30); SH2 – softening hyperelasticity model described by Eq. (27).

where the energy balance is the basis of the theory. The energy nature of LEFM appears in disguise. Indeed, the critical stress intensity factors (SIF) that indicate the onset of fracture are the coefficients in the local asymptotic expansions of stress fields. At first glance, they are not formally related to any energy consideration. However, the stress intensity factors are "truly esoteric quantities" [15] unless they are physically interpreted within the energetic framework of Griffith and the link is established between the critical SIF and the critical energy release rate. Thus, the fracture criteria of LEFM are essentially energetic though they appear in a form related to the local stress. It is remarkable that though the classical theories of brittle fracture ignore the crack sharpness they are capable of describing the influence of the crack length on the critical load very well in the case where the crack sharpness is constant. Our simulations of the straight cracks show that the critical tension depends inversely on the square root of the crack length in full harmony with the Griffith finding.

Considering our simulations it should not be missed that we assume that the crack starts with a massive bond rupture in the process zone at the tip of the crack. This event is volumetric and the use of the softening hyperelasticity is reasonable unless the localized deformation and failure occur at the length scale of the material structure (grains, atomic spacing

Table 3
Normalized critical tension, p_{cr}/Φ, for straight crack with constant yet different sharpness and varying length. SH2 – softening hyperelasticity model described by Eq. (27); small numbers designate the total number of finite elements for the half plate.

a/b	SH2		a/b	SH2		a/b	SH2	
20/1	13.7	13.8	20/2	18.0	18.1	20/3	21.3	21.5
	3746	6202		3200	5644		2942	5222
30/1	11.3	11.4	30/2	15.6	15.7	30/3	18.2	18.2
	3770	6292		3438	6356		3174	5644
40/1	9.9	10.0	40/2	13.4	13.5	40/3	16.1	16.1
	4014	7906		3514	7028		3110	6038
50/1	8.9	9.0	50/2	12.0	12.2	50/3	14.3	14.4
	3996	7972		3870	7864		3252	6928
60/1	8.0	8.2	60/2	11.0	11.1	60/3	13.1	13.2
	4034	8748		4110	8238		3298	7042
70/1	7.4	7.5	70/2	10.2	10.3	70/3	12.4	12.5
	4286	9536		4016	8868		3548	7834
80/1	6.9	7.0	80/2	9.6	9.7	80/3	11.6	11.6
	4306	9422		4180	8942		3568	7956

Table 4
Normalized critical tension, p_{cr}/Φ, for straight crack with constant yet different sharpness and varying length. SH1 – softening hyperelasticity model described by Eq. (27); small numbers designate the total number of finite elements for the half plate.

a/b	SH1		a/b	SH1		a/b	SH1	
20/1	13.2	13.2	20/2	17.5	17.5	20/3	20.3	20.2
	3746	6202		3200	5644		2942	5222
30/1	10.6	10.6	30/2	14.3	14.3	30/3	17.1	17.1
	3770	6292		3438	6356		3174	5644
40/1	9.2	9.1	40/2	12.6	12.7	40/3	15.1	15.2
	4014	7906		3514	7028		3110	6038
50/1	8.2	8.2	50/2	11.4	11.5	50/3	13.7	13.8
	3996	7972		3870	7864		3252	6928
60/1	7.7	7.5	60/2	10.5	10.6	60/3	12.5	12.6
	4034	8748		4110	8238		3298	7042
70/1	7.0	6.9	70/2	9.7	9.7	70/3	11.7	11.8
	4286	9536		4016	8868		3548	7834
80/1	6.5	6.5	80/2	9.1	9.1	80/3	11.0	11.1
	4306	9422		4180	8942		3568	7956

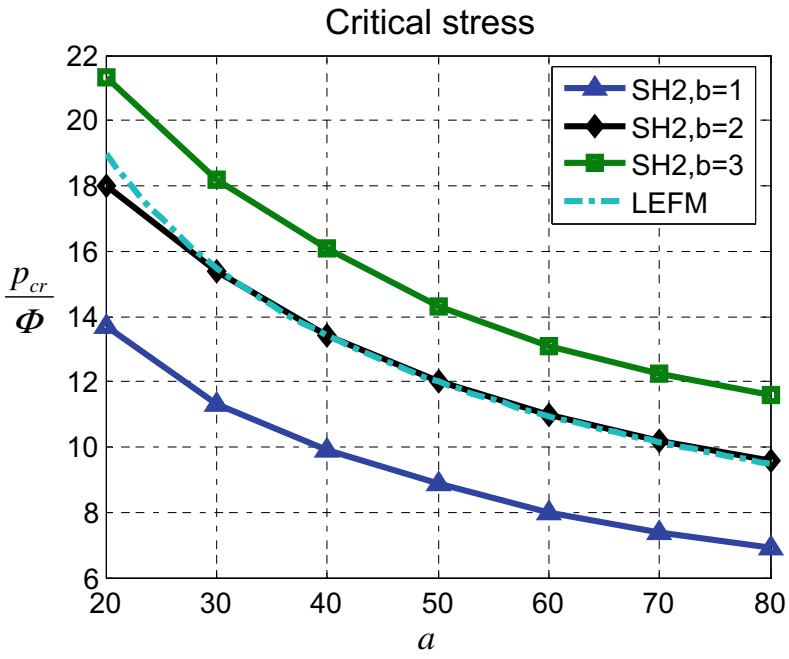

Fig. 7. Critical stress for straight crack with fixed yet different sharpness and varying length. SH2 – softening hyperelasticity model described by Eq. (27). LEFM – prediction based on Eq. (1) for K_{IIc} calibrated at $a/b = 50/2$.

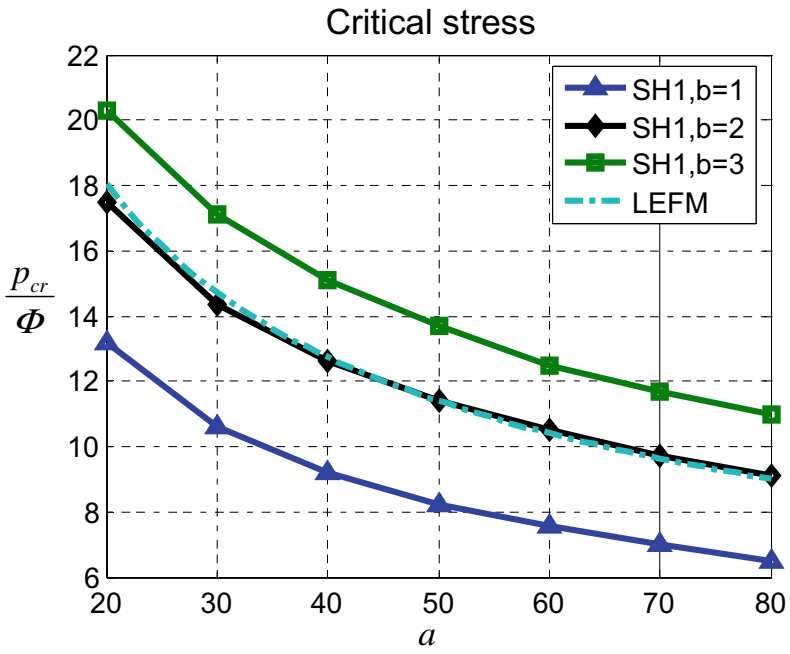

Fig. 8. Critical stress for straight crack with fixed yet different sharpness and varying length. SH1 – softening hyperelasticity model described by Eq. (27). LEFM – prediction based on Eq. (1) for K_{IIc} calibrated at $a/b = 50/2$.

etc). In the latter case the size of the finite elements cannot be decreased beyond the characteristic length of material. This limitation would introduce the characteristic length in analysis implicitly.

The main practical implication of our results is a conclusion that generally the fracture toughness may be difficult to calibrate in experimental tests because its numerical magnitude significantly depends on the sharpness of the crack/notch used for the calibration. The crack sharpness controls the stress/strain concentration, which in turn controls the onset of fracture. It is possible, however, to decrease the radius of the tip of the crack/notch to a magnitude where our conclusion based on the classical continuum considerations is not applicable. Such a magnitude should be related with a characteristic length of the material microstructure, e.g. grain size, atomic distance etc. Concerning the latter remark it is interesting to quote Munz and Fett [24] who notice that the convergence of the measured fracture toughness starts with a notch radius smaller than a critical value: "For a fine-grained ceramic a very narrow notch is necessary. In all cases it has to be ensured that the saw cut is narrow enough". In our opinion, the 'narrow enough' is defined by the grain size. The said is applicable to any sort of brittle materials.

Finally, we would like to emphasize that the interpretation of our results should be cautious. Though LEFM and Griffith ignore the actual sharpness of the real physical cracks they still have a predictive power in the following asymptotic sense. If a true material toughness can be found in experiments, then LEFM and Griffith theories can be used to predict the worst scenario of the onset of the crack propagation in the case when the radius of the crack tip is zero. Of course, the tip radius of real cracks is never zero and, consequently, the critical loads for real cracks are higher than the critical loads for idealized mathematical cracks predicted by Griffith and LEFM. In this sense the error induced by the classical theories generates the safety factor, which is good for engineering. In other words, we can say that the classical theories give the lower bound for the critical loads. All said is valid, again, when the experimentally calibrated fracture toughness is reasonable.

Acknowledgement

This research was supported by the Israeli Ministry of Construction and Housing.

References

[1] Barenblatt GI. The formation of equilibrium cracks during brittle fracture. General ideas and hypotheses. Axially-symmetric cracks. J Appl Math Mech 1959;23:622–36.
[2] Belytschko T, Moes N, Usiu S, Parimi C. Arbitrary discontinuities in finite elements. Int J Num Meth Engng 2001;50:993–1013.
[3] Bertolotti RL. Fracture toughness of polycrystalline Al_2O_3. J Am Ceram Soc 1973;56:107–10.
[4] Broberg KB. Cracks and fracture. London: Academic Press; 1999.
[5] Camacho GT, Ortiz M. Computational modeling of impact damage in brittle materials. I. J Solids Struct 1996;33:2899–938.
[6] De Borst R. Some recent issues in computational failure mechanics. Int J Numer Meth Engng 2001;52:63–95.
[7] Doremus RH. Cracks and energy criteria for brittle fracture. J Appl Phys 1976;47:1833–6.
[8] Dugdale DS. Yielding of steel sheets containing slits. J Mech Phys Solids 1960;8:100–4.
[9] Emmerich FG. Tensile strength and fracture toughness of brittle materials. J Appl Phys 2007;102:073504.

[10] Gao H, Klein P. Numerical simulation of crack growth in an isotropic solid with randomized internal cohesive bonds. J Mech Phys Solids 1998;46:187–218.
[11] Gogotsi GA. Fracture toughness of ceramics and ceramic composites. Ceram Int 2003;7:777–84.
[12] Griffith AA. The phenomena of rupture and flow in solids. Phil Trans Roy Soc London 1921;A221:163–98.
[13] Hellan K. Introduction to fracture mechanics. New York: McGraw-Hill; 1984.
[14] Hertzberg RW. Deformation and fracture of engineering materials. Wiley; 1989.
[15] Hutchinson JW. Life as a mechanician: 1956-. Timoshenko medal acceptance speech: http://imechanica.org/node/195; 2002. .
[16] Inglis CE. Stresses in a plate due to presence of cracks and sharp corners. Proc Inst Naval Architects 1913;55:219–41.
[17] Kachanov LM. Time of the rupture process under creep conditions. Izvestiia Akademii Nauk SSSR, Otdelenie Teckhnicheskikh Nauk 1958;8:26–31.
[18] Kachanov LM. Introduction to continuum damage mechanics. Dotrecht, Netherlands: Martinus Nijhoff; 1986.
[19] Kanninen MF, Popelaar C. Fundamentals of fracture mechanics. London: Butterworth; 1973.
[20] Klein P, Gao H. Crack nucleation and growth as strain localization in a virtual-bond continuum. Engng Fract Mech 1998;61:21–48.
[21] Krajcinovic D. Damage mechanics. Elsevier, North Holland Series in Applied Mathematics and Mechanics; 1996.
[22] Lemaitre J, Desmorat R. Engineering damage mechanics: ductile, creep, fatigue and brittle failures. Berlin: Springer; 2005.
[23] Munz D, Bubsey RT, Shannon JL. Fracture toughness determination of Al_2O_3 using four point bend specimens with straight-through and chevron notches. J Am Ceram Soc 1980;63:300–5.
[24] Munz D, Fett T. Ceramics: mechanical properties, failure behaviour, material selection. Berlin: Springer; 1999.
[25] Myers RJ, Hillberry BM. Effect of notch radius in the fracture behavior of mono-crystalline silicon. In: ICF4 Proceedings, vol. 3. Waterloo, Canada; 1977. p. 1001–5.
[26] Needleman A. A continuum model for void nucleation by inclusion debonding. J Appl Mech 1987;54:525–31.
[27] Rabotnov YN. On the equations of state for creep. In: Progress in applied mechanics (Prager Anniversary Volume). New York: MacMillan; 1963.
[28] Rice JR, Wang JS. Embrittlement of interfaces by solute segregation. Mat Sci Engng A 1989;107:23–40.
[29] Rittel D, Wang ZG, Merzer M. Adiabatic shear failure and dynamic stored energy of cold work. Phys Rev Let 2006;96:075502.
[30] Skrzypek J, Ganczarski A. Modeling of material damage and failure of structures. Berlin: Springer; 1999.
[31] Tadmor EB, Ortiz M, Phillips R. Quasicontinuum analysis of defects in solids. Phil Mag 1996;73:1529–63.
[32] Tvergaard V, Hutchinson JW. The relation between crack growth resistance and fracture process parameters in elastic–plastic solids. J Mech Phys Solids 1992;40:1377–97.
[33] Tsuji K, Iwase K, Ando K. An investigation into the location of crack initiation sites in alumina, polycarbonate and mild steel. Fatigue Fract Engng Mater Struct 1999;22:509–17.
[34] Volokh KY. Nonlinear elasticity for modeling fracture of isotropic brittle solids. J Appl Mech 2004;71:141–3.
[35] Volokh KY. Softening hyperelasticity for modeling material failure: analysis of cavitation in hydrostatic tension. Int J Solids Struct 2007;44:5043–55.
[36] Volokh KY. Hyperelasticity with softening for modeling materials failure. J Mech Phys Solids 2007;55:2237–64.
[37] Volokh KY, Trapper P. Fracture toughness from the standpoint of softening hyperelasticity. J Mech Phys Solids 2008;56:2459–72.
[38] Wang J, Rainforth WM, Wadsworth I, Stevens R. The effects of notch width on the SENB toughness for oxide ceramics. J Eur Ceram Soc 1992;10:21–31.
[39] Weiner JH. Statistical mechanics of elasticity. New York: Wiley; 1983.
[40] Xu XP, Needleman A. Numerical simulations of fast crack growth in brittle solids, J. Mech Phys Solids 1994;42:1397–434.
[41] Yosibash Z, Bussiba A, Gilad I. Fracture criteria for brittle elastic materials. Int J Fract 2004;125:307–33.